Acta Crystallographica Section D
Biological Crystallography
ISSN 0907-4449

Analysis of two polymorphic forms of a pyrido[2,3-*d*]pyrimidine N9—C10 reversed-bridge antifolate binary complex with human dihydrofolate reductase

Vivian Cody,[a]* Nikolai Galitsky,[a] Joseph R. Luft,[a] Walter Pangborn[a] and Aleem Gangjee[b]

[a]Hauptman–Woodward Medical Research Institute Inc., 73 High Street, Buffalo, NY 14203, USA, and [b]Division of Medicinal Chemistry, Graduate School of Pharmaceutical Science, Duquesne University, Pittsburgh, PA 15282, USA

Correspondence e-mail: cody@hwi.buffalo.edu

Received 30 September 2002
Accepted 21 January 2003

PDB References: 2,4-diamino-6-[*N*-(3′,4′,5′-trimethoxybenzyl)-*N*-methylamino]pyrido[2,3-*d*]pyrimidine–hDHFR complex (1), 1mvs, r1mvssf; complex (2), 1mvt, r1mvtsf.

The results of the crystal structure determination of human dihydrofolate reductase (hDHFR) as a binary complex with the potent N9—C10 reversed-bridge antifolate inhibitor 2,4-diamino-6-[*N*-(3′,4′,5′-trimethoxybenzyl)-*N*-methylamino]-pyrido[2,3-*d*]pyrimidine (1) are reported for two independent polymorphic rhombohedral *R*3 lattices [R3(1) and R3(2)]. Data from these two crystal forms were refined to 1.90 Å resolution for complex R3(1), with $R = 0.186$ for 9689 data, and to 1.80 Å resolution for complex R3(2), with $R = 0.194$ for 13 305 data. Changes in the loop geometry between the two structures reflects contact differences in the packing environments in the two *R*3 lattices. The largest changes (between 0.5 and 1.7 Å) are observed for the loop regions encompassing residues 16–25, 40–48, 81–89, 99–108, 143–148 and 161–169. Comparison of the intermolecular contacts of these loops reveals that the R3(2) lattice is more tightly packed, as reflected in its smaller V_M value and smaller solvent content. The conformation of inhibitor (1) is similar in both structures and the N9—C10 bridge geometry is more similar to that observed for the normal C9—N10 bridge of trimetrexate (TMQ) than to the other N9—C10 reversed-bridge antifolates previously reported. The effect of the N9—C10 reversed-bridge geometry is to distort the bridge from coplanarity with the pyrido[2,3-*d*]pyrimidine ring system and to twist the C10 methylene conformation towards a *gauche* conformation. This also influences the conformation of the methoxybenzyl ring, moving it away from a *trans* position and placing the 5′-methoxy group deeper within the hydrophobic pocket made by Leu60, Pro61 and Asn64 of the hDHFR active site.

1. Introduction

Infections with *Pneumocystis carinii* (*pc*) and *Toxoplasma gondii* (*tg*) still present major medical challenges, particularly in patients with immune-compromised conditions such as AIDS (Mills & Masur, 1991). Antifolates have been shown to be effective against dihydrofolate reductase (DHFR) from the *pc* and *tg* pathogens and are therefore of interest as targets for drug-design studies. Despite their limited selectivity against these pathogens, trimethoprim (TMP) and trimetrexate (TMQ) (Fig. 1), weak inhibitors of *pc*DHFR and *tg*DHFR, are used in the treatment of *pc* and *tg* infections (Masur *et al.*, 1993). Of the many antifolates designed to enhance selectivity against these opportunistic pathogens (Gangjee *et al.*, 1996, 1998; Queener, 1995; Piper *et al.*, 1996), biological data for a series of 2,4-diamino-6-(benzylamino)pyrido[2,3-*d*]pyrimidine antifolates with an N9—C10 reversed bridge showed them to be potent and selective inhibitors against *pc*DHFR and *tg*DHFR (Gangjee *et al.*, 1996). Among this series, a pattern of differential inhibitory potencies was observed for N9-methyl

analogs with variable methoxy substitutions (Fig. 1). For example, even though compound (1) has a 230-fold increase in potency against *pc*DHFR and a 25-fold increase against *tg*DHFR over its N9-desmethyl analog (2), it showed a decrease in its *tg*DHFR selectivity (Gangjee *et al.*, 1996). These data are in contrast to the increased potency and selectivity against *pc*DHFR and *tg*DHFR shown by the dimethoxybenzyl pyrido[2,3-*d*]pyrimidine analogs (3) and (4) (Table 1) (Gangjee *et al.*, 1996, 1998).

Sequence alignment of human DHFR (hDHFR), *pc*DHFR and *tg*DHFR indicates the presence of several highly conserved residues and shows that the active-site regions are homologous (Roos, 1993). The most significant differences among these three enzymes is that the acidic active-site residue 30 (human numbering) is Glu in hDHFR and *pc*DHFR but is Asp in *tg*DHFR (Table 2). The hydrophobic character at positions 31 and 60 is conserved despite residue changes between the enzymes. One of the more significant changes involves position 35 (Gln, Lys and Ser, respectively), which is involved in contacts to the conserved Arg70. Structural data reveal that there is subdomain movement of the loop involving residue 35 towards the conserved Arg70 when the inhibitor does not contain a *p*-aminobenzylglutamate moiety (Gangjee *et al.*, 1998; Cody *et al.*, 1999). The strength of the hydrogen-bonding interactions between residue 35 and the conserved Arg70 would be affected by the residue changes between these DHFR enzymes, which could also affect the selectivity of enzyme inhibition.

Table 1
Biological activity data (IC_{50}) and selectivity ratios reported for the antifolates shown in Fig. 1 (Gangjee *et al.*, 1996, 1998).

	IC_{50} (n*M*)			Selectivity ratio	
Analog	*pc*DHFR	rlDHFR†	*tg*DHFR	rlDHFR/*pc*DHFR	rlDHFR/*tg*DHFR
TMP	12000	133000	2700	1.1	49
TMQ	42	3	10	0.07	0.3
(1)	61	33	14	0.5	2.4
(2)	141000	3300	350	0.23	9.4
(3)	84	57	6.3	0.7	9.0
(4)	76	72	31	0.9	2.3
(5)	87	26	30	0.29	0.86

† Rat liver DHFR.

Table 2
Sequence comparison among DHFRs.

Residue (human numbering)	hDHFR	*pc*DHFR	*tg*DHFR
21	Asp	Ser	Gly
30	Glu	Glu	Asp
31	Phe	Ile	Phe
33	Tyr	Tyr	His
35	Gln	Lys	Ser
60	Ile	Ile	Met
64	Asn	Phe	Phe

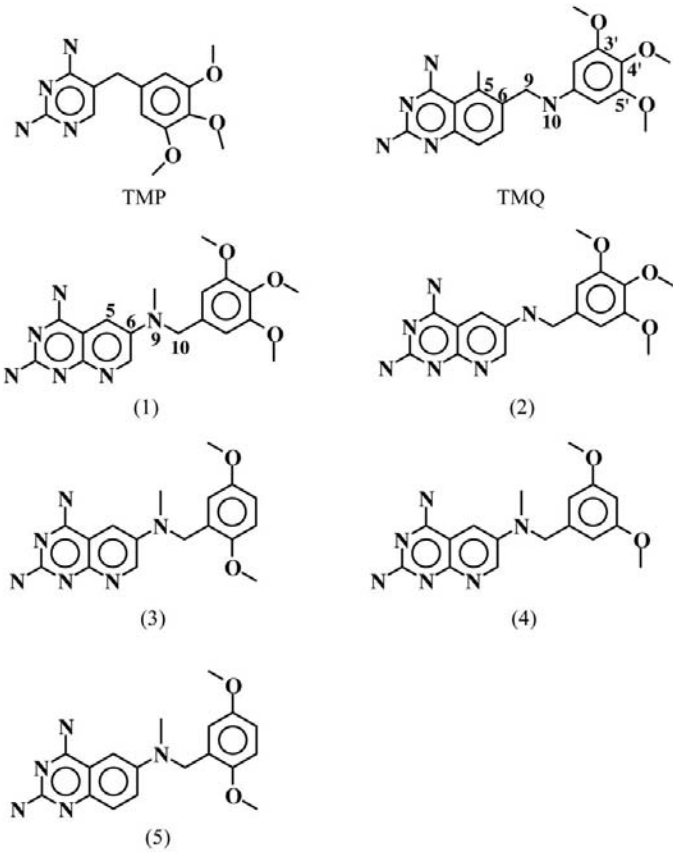

Figure 1
Schematic representation of trimethoprim (TMP), trimetrexate (TMQ) and its 5-desmethyl-pyrido[2,3-*d*]pyrimidine N9—C10 reversed-bridge analogs.

To understand this pattern of potency and selectivity for *pc*DHFR and *tg*DHFR, crystallographic results are reported for the first observation of two polymorphic *R*3 binary complexes of hDHFR and the 3′,4′,5′-trimethoxy-*N*-9-methyl pyrido[2,3-*d*]pyrimidine analog (1) (Fig. 1). These data are compared with previously reported structural complexes of the F31G variant of hDHFR with the 2′,5′-dimethoxy pyrido[2,3-*d*]pyrimidine analog (3) (Gangjee *et al.*, 1998) and *pc*DHFR complexes with compounds (4) and (5) (Cody *et al.*, 2002).

2. Experimental

2.1. Crystallization and X-ray data collection

hDHFR was isolated and purified by Blakley as described in Chunduru *et al.* (1994) and crystals were grown using the hanging-drop vapor-diffusion method. The protein was washed in a Centricon-10 with 100 m*M* KCl, 50 m*M* phosphate buffer pH 6.8. Samples of hDHFR were incubated with NADPH and compound (1) overnight at 277 K. The protein was washed to remove excess inhibitor and cofactor and was concentrated to 10.0 mg ml^{-1}. Protein droplets contained 61% ammonium sulfate in 0.1 *M* phosphate buffer pH 6.8. Crystals grew in three weeks and were rhombohedral, belonging to space group *R*3, and diffracted to 1.9 and 1.8 Å resolution for the polymorphic forms R3(1) and R3(2), respectively. The unit-cell parameters for these binary complexes of hDHFR

Table 3
Crystal properties and refinement statistics.

(*a*) Properties and statistics.

	R3(1) hDHFR–(1)	R3(2) hDHFR–(1)
Unit-cell parameters		
a, *b* (Å)	85.49	106.78
c (Å)	77.61	43.82
Unit-cell volume (Å^3)	491209	432683
V_M (Å^3 Da^{-1})	2.56	2.25
Solvent content (%)	52	42
Space group	*R*3	*R*3
Resolution range (Å)	8.0–1.9	8.0–1.8
R_{merge} (%)	5.6	2.5
Completeness (last shell) (%)	61.2	41.2
Overall completeness (%)	90.6	85.3
No. of reflections used	9689	13305
Total No. of reflections	10689	15377
R factor (%)	18.6	19.4
No. of protein atoms	1502	1502
No. of water molecules	67	42
Residues in most favored region of Ramachandran plot (%)	89.3	89.9
B factor (protein average) (Å^2)	25.7	23.9

(*b*) Distances and torsion angles.

	R.m.s. σ	Target σ	R.m.s. σ
Distances (Å)			
Bonds	0.024	0.020	0.019
Angles	0.061	0.040	0.050
Planar 1–4	0.065	0.050	0.051
Planar groups	0.019	0.025	0.015
Chiral volume	0.210	0.500	0.167
Single torsion	0.229	0.500	0.193
Multiple torsion	0.280	0.500	0.255
Possible hydrogen bonds	0.254	0.500	0.234
Torsion angles (°)			
Planar	3.1	3.0	2.9
Staggered	22.7	15.0	21.5
Orthonormal	24.7	15.0	21.0

are listed in Table 3. Data were collected at room temperature on a Rigaku R-AXIS IIc area detector and were processed with *DENZO* (Otwinowski & Minor, 1997). All data were refined to their resolution limits (Table 3).

2.2. Structure determination and refinement

The structures of both forms of hDHFR–(1) binary complex were solved by molecular-replacement methods and were refined with the restrained least-squares program *PROLSQ* (Hendrickson & Konnert, 1980; Finzel, 1987) in combination with the model-building program *CHAIN* (Sack, 1988). All calculations were carried out on a Silicon Graphics Impact R10000 Workstation. The initial $(2|F_o| - |F_c|)\exp(i\alpha_c)$ maps, where F_o are the observed and F_c the calculated structure factors based on the protein model only and α_c is the calculated phase, resulted in electron density corresponding to the inhibitor but not the cofactor in both structures (Fig. 2). Two sulfate groups from the precipitating agent occupy the pyrophosphate positions of NADPH and water molecules fill the nicotinamide ring pocket in these binary structures.

Further restrained refinement was continued for both binary complexes, including inhibitor and water. Models of (1) were generated from the crystal structure of (3) (Gangjee *et al.*, 1998) and were optimized with *SYBYL* (Tripos Inc., 1997). Between least-squares minimizations, the structure was manually adjusted to fit the difference electron density and was verified by a series of omit maps calculated from the current model with deleted fragments. The final refinement statistics are summarized in Table 3. The Ramachandran conformational parameters from the last cycle of refinement generated by *PROCHECK* (Laskowski *et al.*, 1993) show that between 89 and 90% of the residues have the most favored conformation and none are in disallowed regions for both polymorphic hDHFR binary complexes with (1).

Table 4
Intermolecular contacts (Å) in hDHFR complexes.

Contacts	R3(1) hDHFR–(1)	R3(2) hDHFR–(1)	F31G hDHFR–(3)†	hDHFR–MTX‡
4NH2···O Ile7	2.7	2.7	3.0	2.5
4NH2···OH Tyr121	3.3	3.5	3.5	3.3
4NH2···O Val115	3.3	3.1	3.1	3.0
2NH2···water	3.4	3.3	3.2	3.2
2NH2···OE2 Glu30	2.8	2.8	2.7	2.9
N1···OE1 Glu30	2.9	2.9	3.0	2.6
Glu30 OE1···water	2.8	2.7	—	2.4
Glu30 OE2···O$^\gamma$ Thr136	2.7	2.7	2.7	3.2
Thr136 O$^\gamma$···water	2.5	2.9	2.8	—
Arg70 NH2···Gln35 NE2	2.8	2.6	—	—
Arg70 NH2···O Lys68	3.1	2.9	3.1	2.6
Arg70 NH1···O$^\gamma$ Thr39	3.7	3.5	2.7	3.5
Trp24 NE1···water	3.1	3.4	—	3.2

† Gangjee *et al.* (1998). ‡ Cody *et al.* (1993).

3. Results

3.1. Overall structure

The overall backbone conformations of the two polymorphic *R*3 hDHFR binary complexes with antifolate (1) differ from each other in several of the flexible-loop regions. These changes arise from differences in packing interactions in the two lattices. As illustrated in Fig. 3, polymorph R3(1) is similar to the F31G variant hDHFR–NADPH ternary complex with (3) (Gangjee *et al.*, 1998). The major conformational changes between these polymorphic structures involve movement (0.5–1.7 Å) of loop regions 20 (residues 16–25), 44 (residues 40–48), 84 (residues 81–89), 103 (residues 99–108), 146 (residues 143–148) and 164 (residues 161–169) (Fig. 3). Similar differences in loop conformations, described as the result of ligand-induced changes on cofactor binding, have been reported between inhibitor binary and cofactor ternary complexes of *Escherichia coli* DHFR (Sawaya & Kraut, 1997) and *pc*DHFR enzyme complexes (Cody *et al.*, 1999, 2000). In these cases, the largest changes are in the flap region at loop 20, which opens and closes on cofactor binding.

3.2. Inhibitor binding

The interactions of the pyrido[2,3-*d*]pyrimidine ring of (1) preserve the overall pattern of contacts with invariant residues

in the DHFR active site (Table 4; Fig. 4). As observed in other DHFR complexes with tight-binding ligands (Cody *et al.*, 1992, 1993, 1999; Cody, Galitsky, Luft, Pangborn, Gangjee *et al.*, 1997; Cody, Galitsky, Luft, Pangborn, Rosowsky *et al.*, 1997; Chunduru *et al.*, 1994; Lewis *et al.*, 1995; Oefner *et al.*, 1988; Davies *et al.*, 1990; Klon *et al.*, 2002), a hydrogen-bonding network involving structural water, the conserved residues Thr136, Glu30 and Trp24 and the N1 nitrogen, the 2-amine group and the N8 nitrogen of inhibitor (1) is maintained. Similarly, the inhibitor 4-amino group makes hydrogen-bonding contacts with the conserved residues Ile7 and Tyr121 (Table 4). This network of hydrogen-bonding interactions is characteristic of all crystal structures reported for DHFR complexes (Cody *et al.*, 1999; Sawaya & Kraut, 1997).

Comparison of the polymorphic *R*3 hDHFR binary complexes with inhibitor (1) reveals that the conformation of inhibitor (1) is the same in both complexes (Table 5). These data further show that the conformation of (1) is also more similar to TMQ (Fig. 5*a*), which has a C-methyl and a normal C9—N10 bridge (Cody *et al.*, 1993), than to inhibitor (3) in the ternary complex with F31G hDHFR (Gangjee *et al.*, 1998) or inhibitors (4) and (5) in the *pc*DHFR complexes (Cody *et al.*, 2002) (Fig. 5*b*). The differences between the conformations of (1) and (3) may also reflect the larger active-site volume of the F31G mutant compared with the F31 wild-type structure of hDHFR.

Analysis of the interactions of the methoxy substituents of the benzyl ring of (1) with the other examples of N9—C10 reversed-bridge analogs shows that the 5′-methoxy group of all reversed-bridge analogs makes close contacts to Leu67 and Gln35 in the hDHFR structures (Fig. 4) (Gangjee *et al.*, 1998) and to Phe69 and Leu72 in the *pc*DHFR structures (Cody *et al.*, 2002). These contacts are more compact in the ternary F31G hDHFR complex with (3) than in the two polymorphic *R*3 lattices of the binary complex. This may be a reflection of the differences in orientation of the pyrido[2,3-*d*]pyrimidine ring of these analogs. A comparison of the inhibitor active-site interactions shows that the pyrido[2,3-*d*]pyrimidine ring of (3) (Gangjee *et al.*, 1998) is shifted about 1.1 Å closer to residue Phe34 than in inhibitor (1). This places the 5′-methoxy group of (3) closer to residues Gln35 and Leu67.

As in TMQ, inhibitor (1) has a 4′-methoxy substituent that is not present in compounds (3), (4) and (5) (Fig. 1). In the

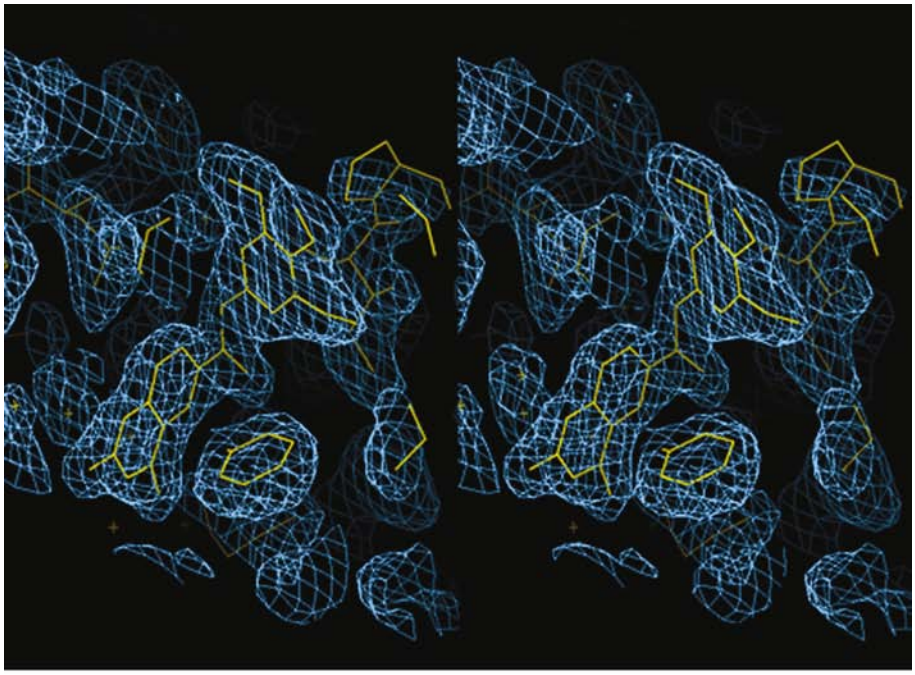

(*a*)

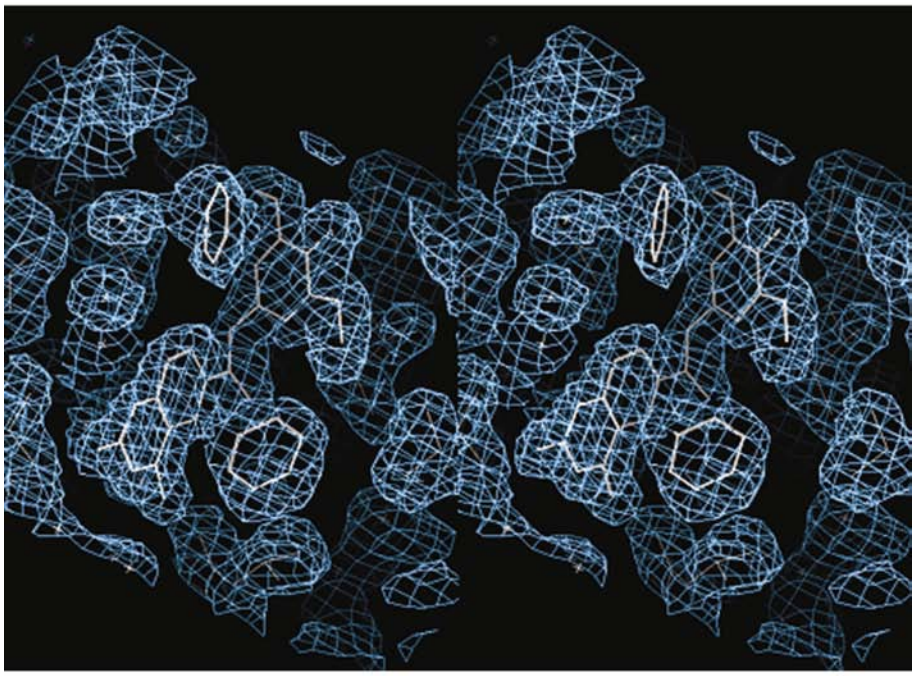

(*b*)

Figure 2
(*a*) Stereoview of $2F_o - F_c$ electron density contoured at 1σ (blue), using phases calculated from only the protein, in R3(1) hDHFR–(1), showing the fit of the enzyme and inhibitor (yellow) to the density. (*b*) Stereoview of $2F_o - F_c$ electron density contoured at 1σ (blue), using phases calculated from only the protein, in R3(2) hDHFR–(1), showing the fit of the enzyme and inhibitor (white) to the density. The diagrams were produced with *CHAIN* (Sack, 1988).

hDHFR–(1) binary complexes, the closest contacts are made with Asn64 (4′-O···N, 3.4 Å) (Fig. 6). This residue is Phe in the *pc*DHFR and *tg*DHFR enzymes (Table 2), which should have more favorable interactions as the 4′-methoxy methyl could also make hydrophobic contacts with Phe69. Since there is a shift in the position of the methoxybenzyl ring of (3) compared with (1), the 5′-O of (3) is displaced in the direction of Asn64 and makes a closer contact than the 5′-methoxy of compound (1) (Fig. 6). This may have an influence on the selectivity of these analogs despite the absence of a 4′-methoxy group in compounds (4) and (5).

Table 5
Bridge torsion angles (°) in DHFR complexes with the analogs shown in Fig. 1.

Structures	C5—C6—N9—C10	C6—N9—C10—C11	N9—C10—C11—C12	C5—C6—N9—CH3
hDHFR–TMQ†	169.1 (C9—N10)	86.1 (C9—N10)	175.9 (C9—N10)	—
R3(1) hDHFR–(1)	157.5	82.4	−163.4	−9.2
R3(2) hDHFR–(2)	158.1	85.5	−166.3	−10.6
F31G hDHFR–(3)‡	170.6	53.3	−138.2	−24.6
*pc*DHFR–(4)§	147.4	77.7	−153.4	−30.8
*pc*DHFR–(5) conf. 1§	−153.9	21.9	−116.9	−0.2
*pc*DHFR–(5) conf. 2§	−90.9	−71.4	−38.9	92.4

† Cody *et al.* (1993). ‡ Gangjee *et al.* (1998). § Cody *et al.* (2002).

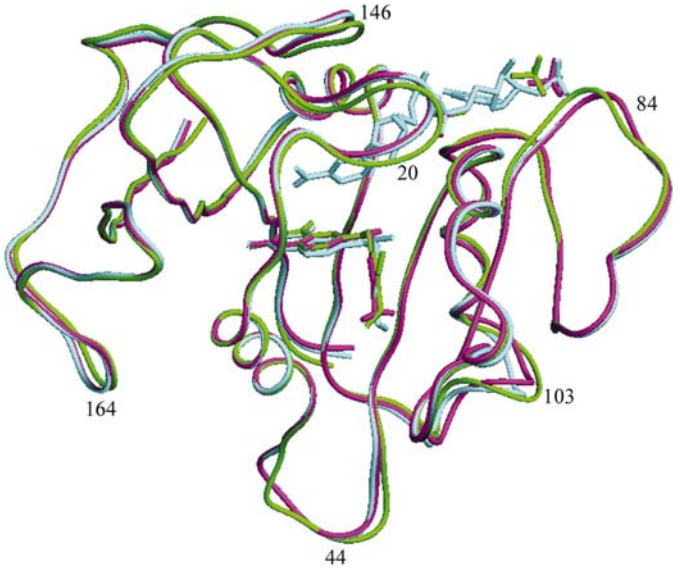

Figure 3
Superposition of the backbone atoms of the R3(1) hDHFR–(1) (violet), R3(2) hDHFR–(1) (green) and F31G hDHFR–NADPH–(3) (cyan) (Gangjee *et al.*, 1998) complexes. Noted on the diagram are the loops that have the largest conformational differences between the two polymorphic *R*3 lattices. Models were produced with *SETOR* (Evans, 1993).

In these structures, the 3′-methoxy group makes a larger number of intermolecular contacts with active-site residues than a methoxy group in the 5′-position. The 3′-methoxy groups of inhibitor (1) make contacts to Asp21, Leu22, Phe31 and Ser59 (Fig. 4); however, many of these contacts are less favorable for the R3(2) lattice, which is more compact. For example, the 3′-methoxy CH_3 of R3(2) makes a C···O contact of 3.2 Å with Asp21. In the case of compound (3), the shift in orientation relative to that of (1) results in the 2′-methoxy group making similar contacts with Asp21 and Leu22.

As a consequence of the changes in bridge geometry of the reversed bridge N9—CH_3, the methyl of these reversed-bridge antifolates probes different regions of the active site than would the N10—CH_3 of the normal bridge in TMQ. For example, in inhibitors (1) and (3), the N9-methyl makes contact with residues Thr56 and Ile60. Again, the contacts are shorter for the R3(2) lattice than the other human DHFR complexes.

It is not clear which factors contribute most to the crystallization of a binary complex in these polymorphic lattices despite the incubation of the enzyme with the cofactor NADPH prior to crystallization. Analysis of the active-site interactions in these polymorphic binary complexes and in the ternary complex hF31G DHFR–NADP–(3) shows that the contact distance between the nicotinamide C2 atom and C5 of inhibitor (3) is 3.9 Å, whereas this distance is 3.5 Å for (1) when modeled in the structure of (3).

3.3. Crystal packing

The observation of two polymorphic *R*3 lattices for the binary complex of hDHFR with compound (1) provides an opportunity to compare the influence of packing interactions on the conformations of surface loops in these structures (Fig. 3). Comparison of the packing arrangements of these two *R*3 lattices (Fig. 7) indicates that the orientation of hDHFR in the R3(1) lattice is such that the helix containing Glu30 is roughly aligned along the crystallographic *c* axis, while in the R3(2) lattice the enzyme is oriented such that this helix is roughly aligned along the *a* axis.

Changes in the orientation of the enzyme in these *R*3 lattices are also reflected by differences in the intermolecular contacts made by the flexible-loop regions in these two

Figure 4
Model of the tertiary structure of the hDHFR–(1) binary complex. Helices are yellow, sheets are magenta, loops are green, inhibitor (1) is red and selected active-site hydrophobic residues are cyan. Models were made with *SETOR* (Evans, 1993).

polymorphs. As illustrated in Table 6, which lists the closest contacts to these loop regions, the R3(2) lattice has a more compact packing environment. This is also reflected in the smaller solvent content of the R3(2) lattice (Matthews, 1968) (Table 3). These data also differ from other *R*3 lattices that were compared with a monoclinic and orthorhombic polymorphic lattice for hDHFR structures (Cody, Galitsky, Luft, Pangborn, Rosowsky *et al.*, 1997).

A more telling difference in the orientation of the enzyme in the two lattices is the packing environment about residue Lys63. In the R3(1) lattice, this residue is situated near the threefold symmetry axis and makes contacts of 4.3 Å to the NZ atoms of the respective side chains. In the R3(2) lattice, this residue does not make any surface contacts with neighboring enzymes; instead, loop 40 is the contact surface closest to the threefold symmetry element. This contact is 8.5 Å for the R3(1) lattice of the hDHFR–NADPH–MTXT ternary complex (Cody *et al.*, 1992), indicating that this structure is more loosely packed (*e.g.* there is more solvent structure in a similar volume).

In a similar manner, the environment around residue Arg32 is another indicator of packing differences. In the R3(1) lattice of the binary complex with (1), this residue is exposed to the solvent channel between molecules. In this environment, the nearest intermolecular contact is to a water molecule (5.1 Å) and to Lys173 (9.2 Å) of the neighboring enzyme. Arg32 forms a short intramolecular hydrogen bond to Gln29 (N···N, 2.4 Å). These contacts are similar for the ternary complex hDHFR–NADPH–MTXT (Cody *et al.*, 1992), where the Arg32 contact to Lys173 is 10.2 Å. The intramolecular contact with Gln29 is 3.2 Å, suggesting that this lattice is less tightly packed. In the R3(2) lattice with (1), Arg32 forms a tight intermolecular hydrogen bond with Glu101 (N···O, 2.6 Å) of a neighboring molecule, while maintaining the conserved intramolecular hydrogen bond with Gln29 (N···N, 2.4 Å). Arg32 was also shown to have close intermolecular hydrogen-bond contacts in the *C*2 and $P2_12_12_1$ lattices of complexes of hDHFR with the potent antifolate PT523 (Cody, Galitsky, Luft, Pangborn, Rosowsky *et al.*, 1997).

Table 6
Intermolecular surface loop packing contacts for human DHFR polymorphs.

Common residue	R3(1) hDHFR–(1) residue	Contact (Å)	R3(2) hDHFR–(1) residue	Contact (Å)	hDHFR–MTXT residue†	Contact (Å)
Asn19	···Ser167	3.4	···Lys54	3.4	···Ser167	3.2
Gly45	···Glu143	10.3	···Ser42	3.2	···Glu143	10.9
Glu78	···Glu150	2.9	···Glu140	3.4	···Glu150	3.5
Pro103	···Gly174	8.0	···Pro160	3.8	···Gly174	8.2
Asp145	···Lys178	4.3	···Phe58	3.5	···Lys178	4.2
Gly164	···Lys108	5.7	···Ser41	3.1	···Lys108	4.2
Ile175	···Pro103	10.9	···Glu78	3.7	···Pro103	11.7

† Cody *et al.* (1992).

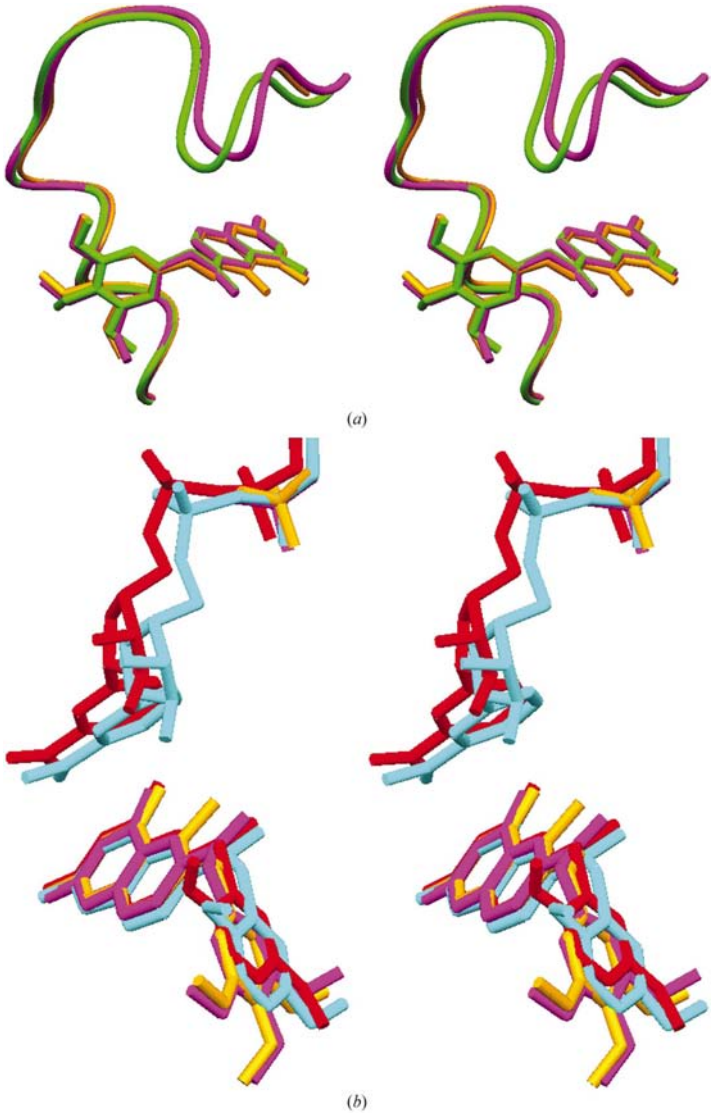

Figure 5
(*a*) Stereo representation illustrating the relative orientation of compound (1) in the binary complex of hDHFR with respect to loop 20 [R3(1), violet; R3(2), green]. Also shown is the orientation of TMQ (gold), which highlights the close similarity in the conformation of TMQ with the reversed-bridge analog (1). Models were made with *SETOR* (Evans, 1993). (*b*) Stereo representation illustrating the superposition of the trimethoxy analog (1) (violet) with that of TMQ (gold) and the 2′,5′-dimethoxy compounds (3) (cyan) and (5) (red) which crystallize as ternary complexes with hDHFR. Models were made with *SETOR* (Evans, 1993).

4. Discussion

This is the first report of two polymorphic rhombohedral forms of hDHFR in a binary complex with an N9—C10 reversed-bridge pyrido[2,3-*d*]pyrimidine analog of TMQ (1). Analysis of the intermolecular packing contacts for these two polymorphic structures reveals that the R3(2) lattice is more tightly packed and that these closer contacts give rise to differences in surface-loop conformations (Fig. 3). The largest conformational changes between these polymorphic lattices are for loops 20 (1.4 Å), 44 (1.5 Å) and 103 (1.7 Å). The close similarity of the loop structure of the ternary complex with F31G hDHFR–NADPH–(3) (Gangjee *et al.*, 1998) (Fig. 3) argues against ligand-induced conformational

changes on cofactor binding as observed for *E. coli* (Sawaya & Kraut, 1997) and *pc*DHFR complexes (Cody *et al.*, 1999). The largest differences between the R3(1) ternary and binary hDHFR structures are in loop 103.

The growth of two polymorphic crystal forms of the *R*3 lattice from nearly identifical crystallization conditions suggests that these two forms are energetically similar and that small changes in the nucleation conditions permits one or the other form to dominate the growth phase. There are no clear indicators in the analysis of the packing interactions of these two polymorphs that indicate which contacts provide the overall advantage of one lattice over another.

The conformation of inhibitor (1) is similar to TMQ, the 5-methyl-trimethoxy parent compound with a C9–N10 bridge, in contrast to the 5-desmethyl *N*-methyl—C10 reverse-bridge variably dimethoxy-substituted inhibitors (3), (4) and (5) (Table 5). These observations suggest that the nature of the bridge and the variability of the bridge geometry among the dimethoxy-substituted inhibitors (3), (4) and (5), compared with the trimethoxy compounds TMQ and (1), are coupled to influence the overall conformation. This would further imply that selectivity of these inhibitors against *pc*DHFR and *tg*DHFR is predicated by sequence-specific ligand interactions (Table 2).

The overall effect of the N9—C10 reversed-bridge geometry is to distort the bridge from coplanarity with the pyrido[2,3-*d*]pyrimidine ring system and to twist the C10 methylene conformation towards a *gauche* conformation. This change also influences the conformation of the methoxybenzyl ring, moving it away from a *trans* position. The flexibility in the N9—C10 reversed-bridge conformation in these inhibitors places the 5′-methoxy group deep within the hydrophobic pocket made by Ile60, Pro61 and Asn64 of the hDHFR active

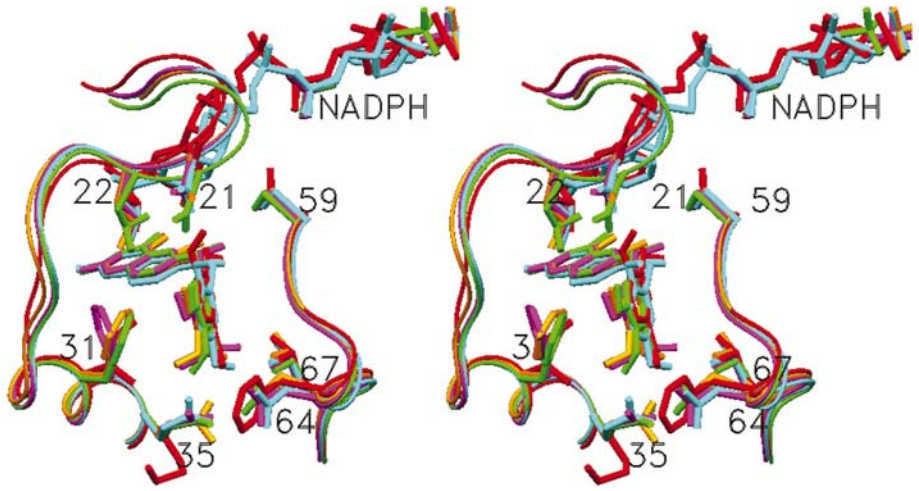

Figure 6
Stereo comparison of the active-site binding region of hDHFR with the N9—C10 reversed-bridge compounds (1) (violet and green), (3) (cyan), (5) (red) and the normal C9—N10 bridge of TMQ (gold). Also highlighted are the active-site residues (human sequence numbering) from both human (violet, green, cyan, gold) and *pc*DHFR (red). As shown in Table 2, the human sequences are Asp21, Leu22, Phe31, Gln35, Ser59, Asn64 and Leu67; the *pc* sequences are Ser24, Leu25, Ile33, Lys37, Ser64, Phe69 and Leu72 (*pc* numbering). The structures containing (3) and TMQ are ternary complexes with NADPH. Models were made with *SETOR* (Evans, 1993).

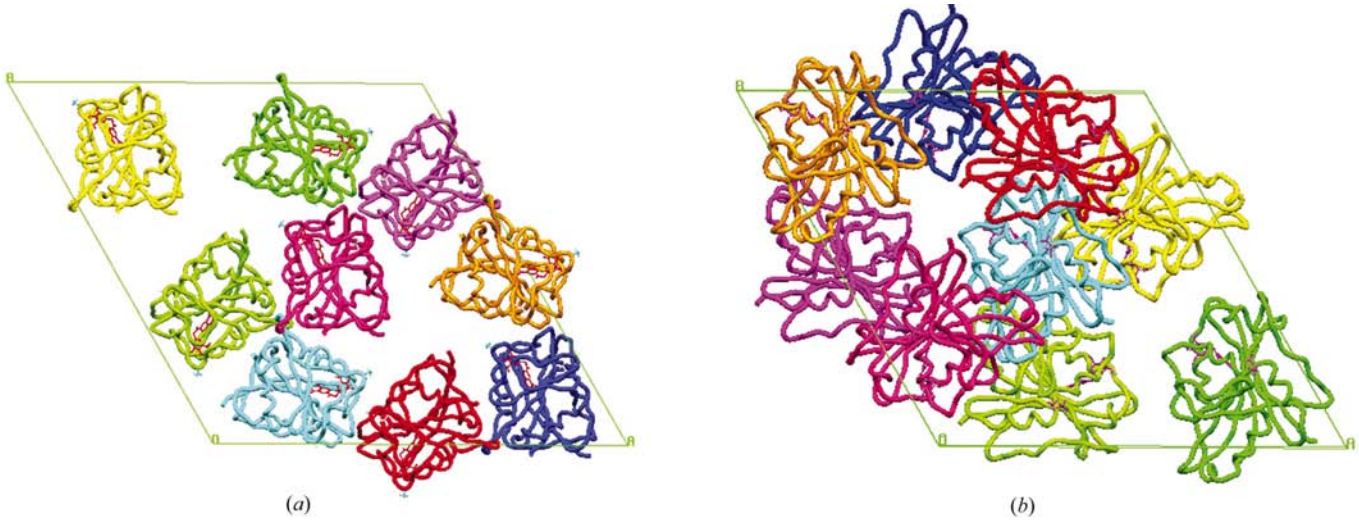

Figure 7
(*a*) Packing arrangement for the R3(1) lattice (outlined in green) projected down the *c* axis for hDHFR–(1) with symmetry-related molecules (x, y, z, pale green; $-y, x-y, z$, green; $y-x, -x, z$, yellow; $x+2/3, y+1/3, z+1/3$, magenta; $-y+2/3, x-y+1/3, z+1/3$, cyan; $y-x+2/3, -x+1/3, z+1/3$, dark blue; $x+1/3, y+2/3, z+2/3$, red; $-y+1/3, x-y+2/3, z+2/3$, gold; $y-x+1/3, -x+2/3, z+2/3$, violet). Inhibitor (1) (red) and residue Lys63 (cyan) are highlighted. (*b*) Packing arrangement for the R3(2) lattice (outlined in green) projected down the *c* axis for hDHFR–(1) with symmetry-related molecules (x, y, z, pale green; $-y, x-y, z$, green; $y-x, -x, z$, yellow; $x+2/3, y+1/3, z+1/3$, magenta; $-y+2/3, x-y+1/3, z+1/3$, cyan; $y-x+2/3, -x+1/3, z+1/3$, dark blue; $x+1/3, y+2/3, z+2/3$, red; $-y+1/3, x-y+2/3, z+2/3$, gold; $y-x+1/3, -x+2/3, z+2/3$, violet). Inhibitor (1) is highlighted in red. Models were made with *SETOR* (Evans, 1993).

site. In the *pc*DHFR enzyme (Table 2), these residues are Ile65, Pro66 and Phe69, thereby changing the nature of the intermolecular contacts. The 3′-methoxy group makes less favorable contacts than the 5′-methoxy with the active-site surface and interacts with Asp21, Leu22 and Phe31. In the *pc*DHFR structure, these residues are Ser24, Leu25 and Ile31, respectively. Structural data for the *pc*DHFR complexes shows that the loop containing Ser24 is further away from the inhibitor compared with the hDHFR structures (Cody *et al.*, 1999), thus enlarging the active site. The mutation of Phe31 to Gly in the F31G hDHFR–NADPH–(3) ternary complex (Gangjee *et al.*, 1998) also provides a greater conformational space for the 2′,5′-dimethoxybenzyl ring compared with wild-type hDHFR or the *pc*DHFR complexes.

These structural studies support the hypothesis that the 5-desmethyl N9—CH_3 reversed-bridge analogs of TMQ have decreased potency and increased selectivity for *pc*DHFR and *tg*DHFR, with the greatest *pc*DHFR selectivity shown for the 3′,5′-dimethoxy TMQ analog (4) and the greatest *tg*DHFR selectivity shown by the 2′,5′-dimethoxy analog (3) (Fig. 1; Table 1). Therefore, the methoxybenzyl ring substitution pattern that interacts with the most highly variable sequences among these DHFR enzymes will have the greatest potential to impact potency and selectivity. This is reflected in the activity differences for inhibitor (1), in which the 3′-methoxy group interacts with variable environments at positions 21 and 31, the 4′-methoxy interacts with variable residues at position 64 and the 5′-methoxy group encounters variable environments at position 35 (Table 2). The greater potency and selectivity of those analogs without a 3′-methoxy group can be ascribed to the removal of unfavorable contacts to Asp21 in the hDHFR structures. This region has a greater conformational space in the *pc*DHFR structures (Cody *et al.*, 1999, 2000) and presumably also in the *tg*DHFR structure since this region has a Gly at this position.

This work was supported in part by the National Institutes of Health grants GM-51670 (VC), AI41743 (AG) and AI44661 (AG).

References

Chunduru, S. K., Cody, V., Luft, J. R., Pangborn, W., Appleman, J. R. & Blakley, R. L. (1994). *J. Biol. Chem.* **269**, 9547–9555.
Cody, V., Chan, D., Galitsky, N., Rak, D., Luft, J. R., Pangborn, W., Queener, S. F., Laughton, C. A. & Stevens, M. F. G. (2000). *Biochemistry*, **39**, 3556–3564.
Cody, V., Galitsky, N., Luft, J. R., Pangborn, W., Gangjee, A., Devraj, R., Queener, S. F. & Blakley, R. L. (1997). *Acta Cryst.* D**53**, 638–649.
Cody, V., Galitsky, N., Luft, J. R., Pangborn, W., Queener, S. F. & Gangjee, A. (2002). *Acta Cryst.* D**58**, 1393–1399.
Cody, V., Galitsky, N., Luft, J. R., Pangborn, W., Rosowsky, A. & Blakley, R. L. (1997). *Biochemistry*, **36**, 13897–13903.
Cody, V., Galitsky, N., Rak, D., Luft, J. R., Pangborn, W. & Queener, S. F. (1999). *Biochemistry*, **38**, 4303–4312.
Cody, V., Luft, J. R., Ciszak, E., Kalman, T. I. & Freisheim, J. H. (1992). *Anticancer Drug Des.* **7**, 483–491.
Cody, V., Wojtczak, A., Kalman, T. I., Freisheim, J. H. & Blakley, R. L. (1993). *Adv. Exp. Biol. Med.* **338**, 481–486.
Davies, J. F., Delcamp, T. J., Prendergast, N. J., Ashford, V. A., Freisheim, J. H. & Kraut, J. (1990). *Biochemistry*, **29**, 9467–9479.
Evans, S. V. (1993). *J. Mol. Graph.* **11**, 134–138.
Finzel, B. C. (1987). *J. Appl. Cryst.* **20**, 53–57.
Gangjee, A., Vasudevan, A., Queener, S. F. & Kisliuk, R. L. (1996). *J. Med. Chem.* **39**, 1438–1446.
Gangjee, A., Vidwans, A. P., Vasudevan, A., Queener, S. F., Kisliuk, R. L., Cody, V., Li, R., Galitsky, N., Luft, J. R. & Pangborn, W. (1998). *J. Med. Chem.* **41**, 3426–3434.
Hendrickson, W. A. & Konnert, J. H. (1980). *Computing in Crystallography*, edited by R. Diamond, S. Ramaseshan & K. Venkatesan, pp. 13.01–13.25. Bangalore, India: Indian Academy of Sciences.
Klon, A. E., Heroux, A., Ross, L. J., Pathak, V., Johnson, C. A., Piper, J. R. & Borhani, D. W. (2002). *J. Mol. Biol.* **320**, 677–693.
Laskowski, R. A., MacArthur, M. W., Moss, D. S. & Thornton, J. M. (1993). *J. Appl. Cryst.* **26**, 283–291.
Lewis, W. S., Cody, V., Galitsky, N., Luft, J. R., Pangborn, W., Chunduru, S. K., Spencer, H. T., Applemann, J. R. & Blakley, R. L. (1995). *J. Biol. Chem.* **270**, 5057–5064.
Masur, H., Polis, M. A., Tuazon, C. V., Ogota, A. D., Kovacs, J. A., Kaz, D., Hilt, D., Simons, F., Feuerstein, I., Lingren, B., Lane, H. C., Chabner, B. A. & Allegra, C. J. (1993). *J. Infect. Dis.* **167**, 1422–1426.
Matthews, B. W. (1968). *J. Mol. Biol.* **33**, 491–497.
Mills, J. & Masur, H. (1991). *Sci. Am.* **263**, 50–57.
Oefner, C., D'Arcy, A. & Winkler, F. K. (1988). *Eur. J. Biochem.* **174**, 377–385.
Otwinowski, Z. & Minor, W. (1997). *Methods Enzymol.* **276**, 307–326.
Piper, J. R., Johnson, C. A., Krauth, C. A., Carter, R. L., Hosmer, C. A., Queener, S. F., Borotz, S. E. & Pfefferkorn, E. R. (1996). *J. Med. Chem.* **39**, 1271–1280.
Queener, S. F. (1995). *J. Med. Chem.* **38**, 4739–4759.
Roos, D. S. (1993). *J. Biol. Chem.* **268**, 6269–6280.
Sack, J. S. (1988). *J. Mol. Graph.* **6**, 244–245.
Sawaya, M. R. & Kraut, J. (1997). *Biochemistry*, **36**, 586–603.
Tripos Inc. (1997). *SYBYL* version 6.0. Tripos Inc., St Louis, MO, USA.